ADVANCED MATERIALS

2000, *287*, 1460. c) M. Ginzburg, M. J. MacLachlan, S. M. Yang, N. Coombs, T. W. Coyle, N. P. Raju, J. E. Greedan, R. H. Herber, G. A. Ozin, I. Manners, *J. Am. Chem. Soc.* **2002**, *124*, 2625. d) Q. Sun, J. W. Y. Lam, K. Xu, H. Xu, J. A. K. Cha, P. C. L. Wong, G. Wen, X. Zhang, X. Jing, F. Wang, B. Z. Tang, *Chem. Mater.* **2000**, *12*, 2617.

[26] For recent work on patterning with magnetic materials, see S. Palacin, P. C. Hidber, J.-P. Bourgoin, C. Miramond, C. Fermon, G. M. Whitesides, *Chem. Mater.* **1996**, *8*, 1316.

[27] F. R. Mayo, *J. Am. Chem. Soc.* **1968**, *90*, 1289.

[28] After this manuscript was submitted, work on the formation of well-organized nanostructured carbon materials based on the carbonization of a phase separated film of a block copolymer of polyacrylonitrile and poly(*n*-butyl acrylate) was described, see T. Kowalewski, N. V. Tsarevsky, K. Matyjaszewski, *J. Am. Chem. Soc.* **2002**, *124*, 10 632.

Laser Pruning of Carbon Nanotubes as a Route to Static and Movable Structures**

By *Kim Yong Lim*, *Chorng Haur Sow*,* *Jianyi Lin*, *Fook Chiong Cheong*, *Ze Xiang Shen*, *John Thiam Leong Thong*, *Kok Chung Chin*, and *Andrew Thye Shen Wee*

Arrays of carbon nanotubes (CNTs) are patterned for applications in microelectronics,[1] field emission,[2] and scanning-probe applications.[3] Typical patterning methods often involve conventional lithographic techniques, resulting in a pre-patterned substrate on which the arrays of nanotubes can be grown.[4–6] Here, we report a simple focused laser beam pruning method to fabricate unique two- and three-dimensional (2D and 3D) static structures without a pre-patterned substrate and under ambient conditions. In addition, by exploiting the elastic nature of CNTs, microscopic, 3D, movable CNT structures, readily controlled by laser light, were constructed. The technique allows for a wider range of three-dimensional CNT microstructures to be constructed. It could also be useful for potential micro-optomechanical and field emission device applications.

Plasma-enhanced chemical vapor deposition (PECVD) was first employed to grow arrays of aligned CNTs on silicon or quartz substrates using iron nanoparticles as catalysts. Details on the growth of the CNTs were reported elsewhere.[7] Each sample was placed in an optical microscope-focused laser-beam system. When the focused beam was incident upon the sample, it caused localized burning of CNTs. By moving the sample with respect to the focused laser beam, patterns of the desired design were created on the CNT-covered surface. Figure 1 shows a schematic of the experimental set-up. The laser beam was directed into the microscope via two reflecting mirrors (M1 and M2). Inside the microscope, the beam was directed towards an objective lens (L) via a beam splitter (S1). A second beam splitter (S2) was used for directing illumination light from an illumination lamp. Depending on whether S2 was engaged or not, the power of the laser beam after passing through the M1–M2–S1–S2 set-up was measured to be 13 mW or 26 mW respectively. The laser beam was then focused by the objective lens (L). The sample was placed on a computer-controlled, motorized X–Y stage.

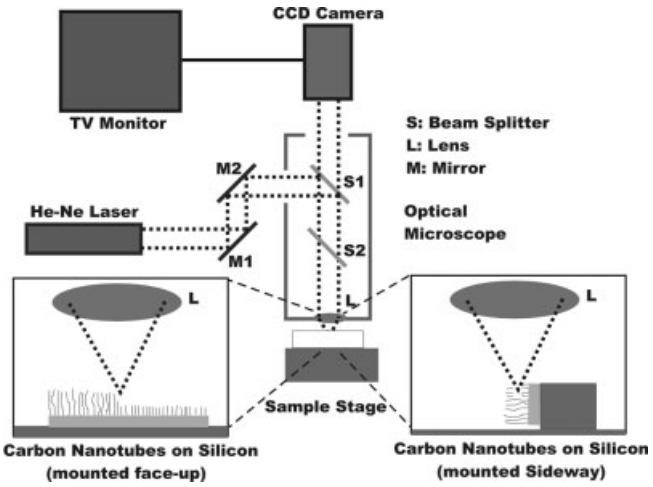

Fig. 1. Schematic of the optical microscope-focused laser beam system used in this work.

During the cutting of the CNTs, the same objective lens (L) was used to collect reflected light from the sample for viewing purposes. The reflected light from the sample passed through the beam splitters S1 and S2 before the light was collected by a charge-coupled device (CCD) camera that was coupled to a monitor. In this way, we could inspect the structures created and move the lens to focus the laser beam to different levels.

The laser exits the laser system with a beam diameter of $w_o = 1.24$ mm. The laser can be focused down to a beam diameter given by[8]

$$w(z) = \frac{4fw_o}{3z} \quad (1)$$

where $f = 0.6$ mm, the focal length of the lens, and $z = 1$ m, the distance the laser traveled from its exit from the laser system to the entry of the objective lens. $w(z)$ is calculated to be 1.0 ± 0.1 μm. This is consistent with the observed cut spot size of 1 μm. However, a faster scan speed can achieve a narrower effective burn width of 600 nm due to the Gaussian profile of the focused laser beam and the shorter exposure time of the CNTs.

The CNTs can be trimmed from either their tips when the laser beam is normal to the sample surface (face-up), or across the cylindrical tubes by mounting the sample sideways (Fig. 1). A laser power of 26 mW was used for the latter, while a 13 mW laser beam was sufficient for the former. This suggests that the cylindrical caps are more reactive than the cylindrical section of the CNTs. This could be due to the pres-

[*] Dr. C. H. Sow, K. Y. Lim, Dr. J. Lin, F. C. Cheong, Dr. Z. X. Shen, K. C. Chin, Dr. A. T. S. Wee
Department of Physics, Faculty of Science
National University of Singapore
2 Science Drive 3, Singapore 117542 (Singapore)
E-mail: physowch@nus.edu.sg
Dr. J. T. L. Thong
Center for Integrated Circuit Failure Analysis and Reliability
Faculty of Engineering, National University of Singapore
4 Engineering Drive 3, Singapore 117576 (Singapore)

[**] The authors acknowledge the support of the NUS Academic Research Fund and the NUS Nanoscience and Nanotechnology Initiative.

  0935-9648/03/0302-0300 $ 17.50+.50/0

ence of exposed pentagons and the greater curvature and reactivity of the caps.

By using samples with short CNT growth, direct writing of the CNT arrays with the focused laser beam resulted in 2D structures (Fig. 2A), with the substrate exposed over the cut areas. To construct 3D structures, we used CNT arrays with longer tubular lengths of about 30 μm. We first focused the laser onto the surface and removed a thin layer of CNTs from the top, after which we moved the objective lens closer to the sample by focusing onto the freshly cut layer. Another thin layer of a different pattern was scanned and removed at this level. This process was repeated successively until the desired structures were created. Figure 2B shows a structure made of different tubular lengths of CNTs within the same sample.

Using a combination of face-up and sideways trimming, it was possible to create structures that are not possible to fabricate using conventional lithographic techniques. For example, Figure 2C shows a horizontal column of aligned CNTs supported in mid-air by a pillar of CNTs, forming an inverted "L" shape. Figure 2D shows that arbitrary 3D structures can be constructed by the same technique utilizing both normal and sideways laser cutting.

Aside from creating 3D static structures, movable flaps of CNTs could also be constructed using this technique. Parallel flaps of freestanding aligned nanotubes were created by focusing a 26 mW laser beam normally onto a sample mounted in the face-up manner. The spread of the beam causes undercutting of the CNT sidewalls, resulting in flaps of CNTs having a narrow base with relatively fewer strands of nanotubes as compared to the top. Figure 3A shows the top view of a pair

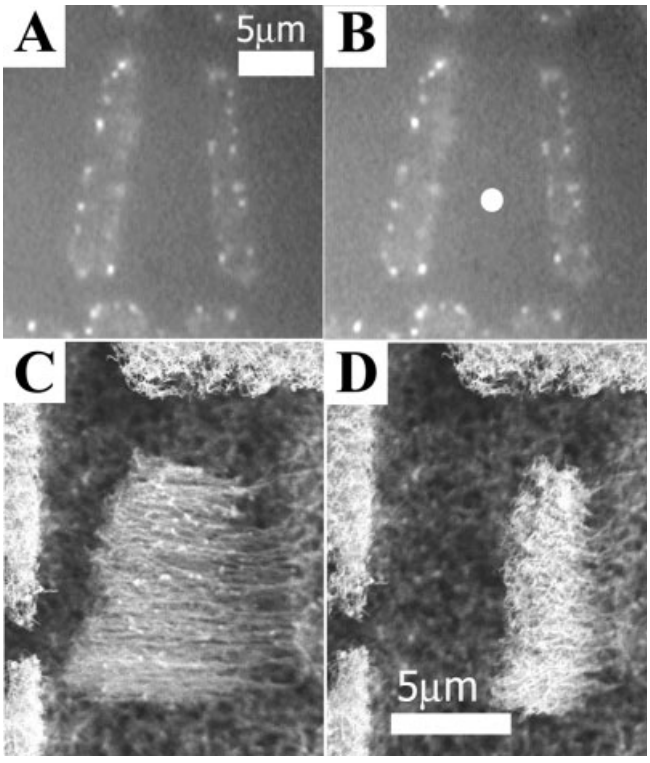

Fig. 3. A) Optical microscope images of the top view of two CNT flaps. B) When a laser beam of 13 mW was focused between the two flaps as indicated by the spot, the two flaps deflected away from the spot. C) SEM image of a flap of CNTs after it was collapsed by a laser beam of power 26 mW focused to the right, and D) the same flap after it was resurrected by laser light focused to the left. Video clips of both processes can be found in the supplementary material [9].

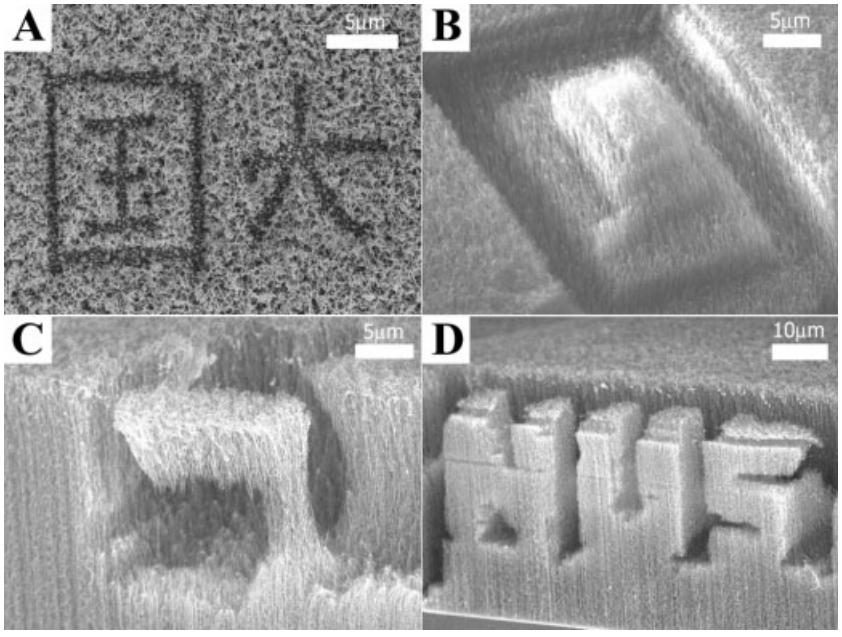

Fig. 2. A) Scanning electron microscope (SEM) images of Chinese characters cut in 2D on a mat of carbon nanotubes. B) A pyramidal structure cut by focusing the laser to different depths and scanning over the pre-determined areas. C) An inverted "L", and D) 3D letters "NUS" are structures produced in a two-step process: cutting first from the side and then with the sample in the face-up configuration.

of parallel flaps created in this way. When a laser beam was focused at a spot mid-way between the parallel flaps with the sample mounted in the face-up position, the flaps were found to deflect away from the focused spot as shown in Figure 3B. When the laser was blocked, the flaps were found to return to their original positions promptly due to the elastic nature of the CNTs. Shifting the focused laser spot to the left or right of the flaps resulted in distinctly different modes of movements as the flaps always deflected away from the light. By blinking the laser light, the CNTs can be made to "dance". Such movements are more clearly illustrated in the supplementary material.[9] This technique can be extrapolated to configurations of more flaps with more laser spots controlling them.

The mechanism for the deflection of the flap is still under investigation, and it is possible that photon pressure is responsible for the deflections of the CNT flaps. The CNT flaps were always found to deflect away

  0935-9648/03/0302-0301 $ 17.50+.50/0

ADVANCED MATERIALS

from the focused laser spot. This was in contrast to the observations by Zhang and Iijima,[10] where filaments of CNTs were found to deflect both towards and away from a light source, and where electric effects were found to be responsible for such responses of CNTs to light. In addition, in our case the deflection of the CNT flaps occurred when they were narrower at the base than at the top. When flaps with similar widths at the base and at the top were created, these flaps could not be deflected from the focused laser spot. Hence, differential expansion of the sides of the CNT flaps due to inhomogeneous heating is unlikely to be a reason for the deflections of the CNT flaps.

While 13 mW was enough to bring about such motions, in a separate experiment, a higher beam power of 26 mW was found to be able to collapse the flap as shown in Figure 3C. The flaps remained collapsed after the removal of the beam. It was presumably held in position by physical entanglement between the flap CNTs and the background CNTs. However, the flap could be resurrected by focusing the laser on the opposite side of the flap with respect to the initial spot (Fig. 3D). The action of collapsing and resurrection of the CNT flap were repeated to ensure robustness. Video clips of the processes can be found in the supplementary material.[9] A scanning electron microscopy (SEM) picture (Fig. 4A) reveals a substantial extension of the CNTs after the flap had collapsed. When it was resurrected (Fig. 4B), the CNTs contracted to their original lengths. The length estimates were made by observing the positions of bright spots in SEM images in the original, collapsed, and resurrected positions. It can also be seen from the SEM pictures that some of the nanotubes were strained upon collapse of the flap. A frame by frame analysis of the movements revealed that the CNTs flap moved from a collapsed position to an upright position within just one frame as recorded by the CCD camera. As the time between successive frames is 40 ms, it can be deduced that such a move has taken less than 40 ms.

CNTs that had been trimmed from their tips also have their tip structures slightly altered. Before trimming, it was observed that, despite the general alignment of the CNTs, the top region of CNTs was not very well-aligned (Fig. 5A). After trimming, there was an improvement in the alignment of the CNTs (Fig. 5B). In addition, nanotubes were fused together at the ends to form multi-junctions. Each junction was made of four or five nanotubes fused together, and was capped with an iron nanoparticle. This was confirmed by SEM pictures taken of a trimmed region in the back-scattered electron (BSE) mode

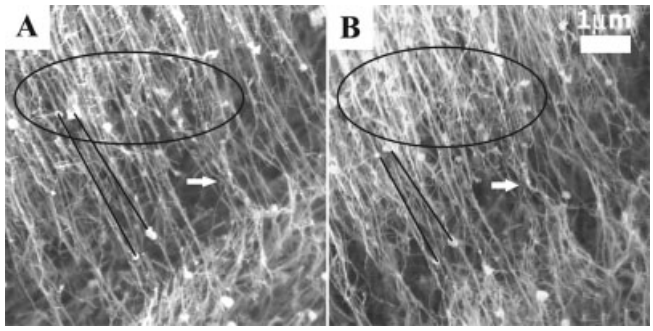

Fig. 4. SEM images of a close-up of the base of the flap when the flap was A) collapsed and B) resurrected. (A) shows strained and elongated carbon nanotubes while (B) shows them in a relaxed state upon resurrection. The lines are an indication of the lengths of the nanotubes between two bright spots chosen A) before and B) after resurrection. The arrow shows a relaxed CNT segment in (B), and the same segment in a stretched position in (A). The CNTs in the oval are visibly stretched in (A) but relaxed in (B).

(Fig. 5E). The bright spots in Figure 5E show positions comprising of a heavier element, presumably iron, since the sample surface is comprised of only carbon and iron. They correspond exactly to the junctions in the SEM micrograph (Fig. 5D) (taken in the secondary electron mode) of the trimmed regions. By assuming that the melting of iron nanoparticles preceded the formation of a junction, the local tem-

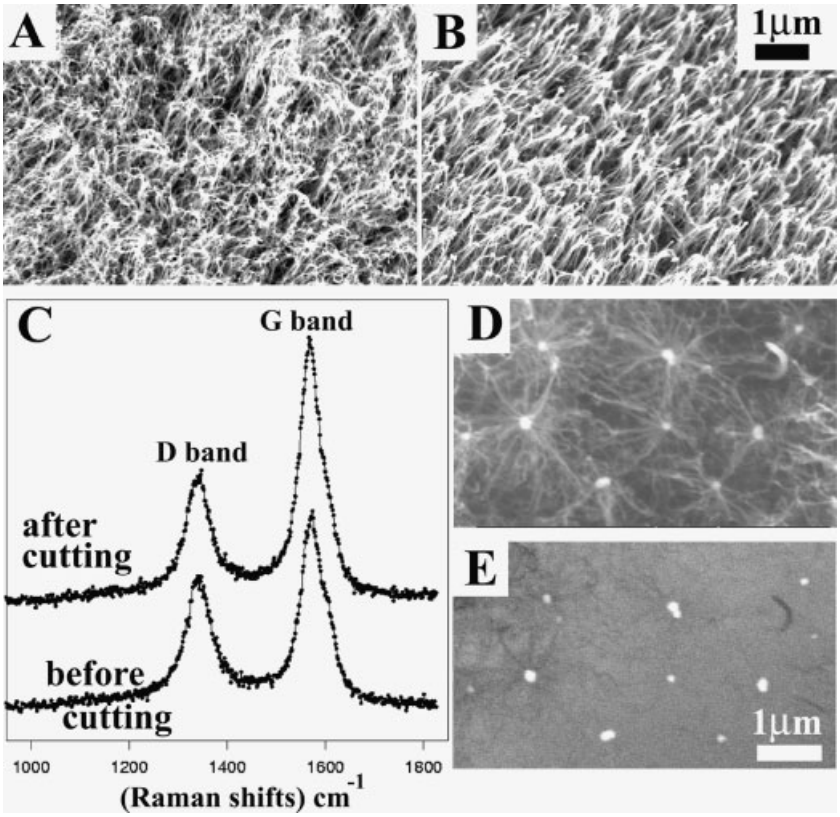

Fig. 5. A) SEM image of the surface morphology of the as-synthesized CNTs. B) An improved alignment of the CNTs and the creation of fused junctions after a thin layer is removed by laser. C) The Raman spectra of the CNTs before and after cutting by laser. D) SEM image of the fused tips after laser cutting. E) Back-scattered electron image of the same area as shown in (D). The bright spots in (E) signify the heavier element, Fe, and they match very well with the fused spots in (D).

  0935-9648/03/0302-0302 $ 17.50+.50/0

perature during laser pruning has a lower bound of 1750 K, as suggested by the liquid-drop model for the size-dependent melting of nanoparticles.[11] The melting temperature of iron nanoparticles, T_m, is given by

$$T_m = T_{mb}(1 - \frac{\beta}{d}) \quad (2)$$

where $T_{mb} = 1809$ K,[11] the melting temperature of bulk iron, $\beta = 0.942$ nm,[11] a constant dependent on the atomic volume and the coefficient of surface energy of iron, and $d \approx 30$ nm, the diameter of the iron nanoparticles.

Raman spectroscopy was also performed on both the cut and uncut regions. Both regions displayed the disordered D- and G-bands at 1348 cm^{-1} and 1566 cm^{-1}, respectively. The former arose from structural disorder in the CNTs, and the latter corresponded to the E_{2g} mode in graphitic material. From the spectra in Figure 5C, the cut regions displayed a lower D- to G-peak intensity ratio than the uncut regions. This shows that a lower degree of structural disorder exists after the CNTs were cut. This behavior is similar to a previous report of laser treatment on single-walled CNTs.[12]

Our laser-pruning method was useful in determining the mechanism of growth of CNTs. Patterns were first cut on pristine well-aligned CNTs near the edges of the sample (Fig. 6A). The sample was then subjected to similar conditions for the growth of an additional layer of CNTs.[7] Figure 6B shows the result after this process. The original patterns were lifted by continued growth of CNTs at the base of the original CNTs. A boundary that separated the two stages of growth was clearly visible and the patterns remained similar after re-growth. There was no observable further growth of CNTs at the tips during the second stage of growth. This points to a predominantly root-growth mechanism in the PECVD growth of CNTs in our samples.

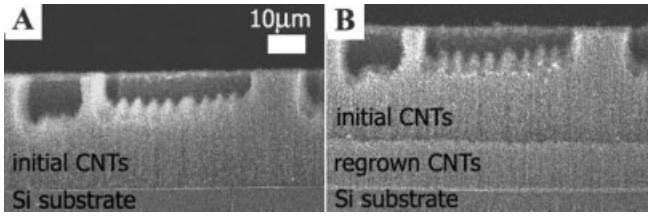

Fig. 6. A) shows aligned CNTs (1200 s of PECVD growth time) of length 34 μm, with patterns created by laser-pruning. B) Root growth upon continued growth of the CNTs under similar conditions (600 s of growth time during continued growth). An additional layer of aligned CNTs of 12 μm length was grown from the silicon substrate. This displaced the first generation of CNTs upwards.

The technique of laser pruning facilitates the fabrication of a wider range of structures on microscopic scales. Different architectures that demand aligned nanotubes of different lengths on the same platform can be fabricated. This could be useful for the fabrication of novel field-emission devices. Also, movable and flexible CNTs microstructures can be constructed. Observations of light-induced movements of arrays of CNTs can potentially be useful in making optomechanical switches.

Experimental

Growth of Arrays of CNTs: Iron nanoparticles were first deposited on silicon or quartz substrate by means of radio frequency (rf) magnetron sputtering. The iron nanoparticles were then reduced by hydrogen plasma to metallic iron particles. A mixture of C_2H_2 and H_2 gases, with a flow rate of 15 sccm (standard cubic centimeters per minute) and 60 sccm respectively, were then introduced at a temperature of 750 °C, a pressure of 1200 mtorr, and an rf plasma of 100 W. The arrays grew perpendicularly to the surface, were of uniform height, and were 30 nm in diameter. In this work, samples of CNTs ranging from 1 μm to 35 μm were used.

Optical Microscope Focused Laser Beam Set-up: In our optical microscope set-up, we used a modified upright microscope in reflection mode. The objective lens used for focusing was an Olympus MDPlan 150× lens with a numerical aperture of 0.95. The sample stage used was a DynaOptic Motion CTC-512-2 XY stage with 25 mm travel and a minimum step size of 50 nm in the *x*- and *y*-directions. It was controlled by a CTC-290-10X motor controller and interfaced to the computer via the Motion Control API software. The laser used was a Melles Griot HeNe laser ($\lambda = 632.8$ nm) with beam divergence of 0.65 mrad, a beam width of 1.24 mm, and a measured power of 30 mW. A wv-CL350 Panasonic CCD camera was used to capture the optical images.

Scanning Electron Microscope Imaging: After the laser-cutting process, scanning electron microscope (SEM) images of the sample were taken using a JEOL JSM-6400F field emission scanning electron microscope system operating at 5 kV. Pictures of the cut region in the back-scattered electron (BSE) mode were taken using a Philips FEG XL-30 model scanning electron microscope.

Raman Spectroscopy: A Renishaw 1000 Raman spectroscope equipped with a charge coupled device detector, operating at a wavelength of 514.5 nm and a power of 100 mW was employed in our experiment. The laser spot was focused on an area of 15 μm^2 by a 50× objective, and with a power of about 5 mW at the sample. The signal was integrated over 5×20 s.

Received: August 14, 2002
Final version: December 3, 2002

[1] R. Martel, T. Schmidt, H. R. Shea, T. Hertel, P. Avouris, *Appl. Phys. Lett.* **1998**, *73*, 2447.
[2] W. A. de Heer, A. Chatelaine, D. Ugarte, *Science* **1995**, *270*, 1179.
[3] H. Dai, J. H. Hafner, A. G. Rinzler, D. J. Colbert, R. E. Smalley, *Nature* **1996**, *384*, 147.
[4] Z. F. Ren, Z. P. Huang, D. Z. Wang, J. G. Wen, J. W. Xu, J. H. Wang, L. E. Calvet, J. Chen, M. A. Reed, J. F. Klemic, *Appl. Phys. Lett.* **1999**, *75*, 1086.
[5] K. B. K. Teo, M. Chhowalla, G. A. J. Amaratunga, W. I. Milne, D. G. Hasko, G. Pirio, P. Legagneux, F. Wyczisk, D. Pribat, *Appl. Phys. Lett.* **2001**, *79*, 1534.
[6] B. Q. Wei, R. Vajtai, Y. Jung, J. Ward, R. Zhang, G. Ramanath, P. M. Ajayan, *Nature* **2002**, *416*, 495.
[7] Y. H. Wang, J. Lin, C. H. A. Huan, G. S. Chen, *Appl. Phys. Lett.* **2001**, *79*, 680.
[8] *The Practical Application of Light*, Melles Griot, Carlsbad, CA **1999**, Ch. 1.
[9] http://www.physics.nus.edu.sg/~physowch/dancingCNT/dancingCNT.html
[10] Y. Zhang, S. Iijima, *Phys. Rev. Lett.* **1999**, *82*, 3472.
[11] K. K. Nanda, S. N. Sahu, S. N. Behera, *Phys. Rev. A* **2002**, *66*, 013 208.
[12] L. Zhang, H. Lin, K. T. Yue, S. L. Zhang, X. Wu, J. Zi, Z. Shi, Z. Gu, *Phys. Rev. B* **2002**, *65*, 073 401.

A Novel Method for Preparing Copper Nanorods and Nanowires

By *Zongwen Liu** and *Yoshio Bando*

Among all metal wires, copper (Cu) wire is the most commonly used one. From electric power leads to interconnects in electronic circuits, copper plays the role that no any other

[*] Dr. Z. Liu, Prof. Y. Bando
Advanced Materials Laboratory
National Institute for Materials Science
Namiki 1-1, Tsukuba, Ibaraki 305-0044 (Japan)
E-mail: liu.zongwen@nims.go.jp

  0935-9648/03/0302-0303 $ 17.50+.50/0